

Discovery of X-ray pulsations in the Be/X-ray binary IGR J21343+4738

P. Reig^{1,2*}, A. Zezas^{2,1}

¹ IESL, Foundation for Research and Technology-Hellas, GR-71110 Heraklion, Crete, Greece

² Institute of Theoretical & Computational Physics, University of Crete, PO Box 2208, GR-710 03, Heraklion, Crete, Greece

Accepted ??, Received ??, in original form ??

ABSTRACT

We report on the discovery of X-ray pulsations in the Be/X-ray binary IGR J21343+4738 during an XMM-Newton observation. We obtained a barycentric corrected pulse period of 320.35 ± 0.06 seconds. The pulse profile displays a peak at low energy that flattens at high energy. The pulse fraction is $45 \pm 3\%$ and independent of energy within the statistical uncertainties. The 0.2–12 keV spectrum is well fit by a two component model consisting of a blackbody with $kT = 0.11 \pm 0.01$ keV and a power law with photon index $\Gamma = 1.02 \pm 0.07$. Both components are affected by photoelectric absorption with a equivalent hydrogen column density $N_H = (1.08 \pm 0.15) \times 10^{22} \text{ cm}^{-2}$. The observed unabsorbed flux is $1.4 \times 10^{-11} \text{ erg cm}^{-2} \text{ s}^{-1}$ in the 0.2–12 keV energy band. Despite the fact that the Be star’s circumstellar disc has almost vanished, accretion continues to be the main source of high energy radiation. We argue that the observed X-ray luminosity ($L_X \sim 10^{35} \text{ erg s}^{-1}$) may result from accretion via a low-velocity equatorial wind from the optical companion.

Key words: X-rays: binaries – stars: neutron – stars: binaries close – stars: emission line, Be

1 INTRODUCTION

IGR J21343+4738 was discovered by the *INTEGRAL*/IBIS in December 2002 (Krivonos et al. 2007; Bird et al. 2007). The IBIS all-sky hard X-ray survey showed that IGR J21343+4738 went through active (December 2002–February 2004) and inactive (Marh 2004–February 2007) periods of X-rays. The mean X-ray flux during the active period was $(2.3 \pm 0.4) \times 10^{-11} \text{ erg cm}^{-2} \text{ s}^{-1}$ in the 17–60 keV band (Bikmaev et al. 2008). In addition to the *INTEGRAL* data, there is only one more detection of IGR J21343+4738 by an X-ray mission. A short 3.4 ks *Chandra* observation of IGR J21343+4738 was made in December 2006, that is, when the X-ray emission was below the threshold of the *INTEGRAL* instruments (Sazonov et al. 2008). Although the source was clearly detected, the low statistics prevented any detailed timing or spectral analysis. However, the *Chandra* observation allowed the refinement of its X-ray position and the identification of the optical counterpart (Sazonov et al. 2008; Bikmaev et al. 2008).

The association of IGR J21343+4738 with a Be star identifies this source as a Be/X-ray binary (BeXB). In this type of X-ray binaries, the normal stellar component is an Oe or Be star that show spectral lines in emission, while the X-ray emitting component is a strongly magnetised neutron star (Reig 2011). Most BeXB are transient sources with episodes of violent eruption in X-rays that may reach luminosities of the order of $10^{38} \text{ erg s}^{-1}$. However, lower

luminosity, less variable BeXB also exist. Transient BeXB usually have short spin ($P_{\text{spin}} \lesssim 100 \text{ s}$) and orbital periods ($P_{\text{orb}} \lesssim 100 \text{ d}$). Low-luminosity BeXB are normally persistent sources and tend to have longer spin periods ($P_{\text{spin}} \gtrsim 100 \text{ s}$) and wider orbits ($P_{\text{orb}} \gtrsim 100 \text{ d}$). Exceptions also occur, such as SAX J2103.5+4545 (Hulleman, in ’t Zand & Heise 1998; Baykal, Stark & Swank 2000) and 1A 0118-616 (Ives, Sanford & Bell Burnell 1975; Staubert et al. 2011), which display long pulsation periods (351 s and 406 s, respectively) and short orbital periods (12.7 d and 24 d, respectively) and thus do not follow the well-known $P_{\text{spin}} - P_{\text{orb}}$ relationship (Corbet 1984). Although the identification of IGR J21343+4738 as a BeXB is firm, neither the orbital or pulse periods are known.

The nature and optical variability of the massive companion has been amply investigated by Reig & Zezas (2014). They found that the optical counterpart to IGR J21343+4738 is a $V = 14.1$ BIIVe shell star located at a distance of $\sim 8.5 \text{ kpc}$. The long-term optical variability is characterised by asymmetric spectral $H\alpha$ line profiles and significant intensity variability. The changes in the strength of the line are associated with the formation and dissipation of a circumstellar disc, while those affecting its shape are believed to be caused by a density perturbation precessing in the disc. The massive companion in IGR J21343+4738 is only the second Be shell¹ star in a BeXB.

* E-mail: pau@physics.uoc.gr

¹ The other one is 4U 1258–61 (Parkes, Murdin & Mason 1980). Be shell

In this work, we analyse the first *XMM-Newton* observations of IGR J21343+4738 during a low optical state and report the discovery of X-ray pulsations with a spin period of 320 s.

2 OBSERVATIONS AND DATA ANALYSIS

2.1 XMM-Newton observations

IGR J21343+4738 was observed by *XMM-Newton* on 2013 November 24 during revolution 2557. The observation (ObsID 0727961301) started at 18:56 hr UT and lasted for ~ 30 ks. The *XMM-Newton* Observatory (Jansen et al. 2001) includes three 1500 cm² X-ray telescopes each with an European Photon Imaging Camera (EPIC) at the focus. Two of the EPIC imaging spectrometers use MOS CCDs (Turner et al. 2001) and one uses PN CCDs (Strüder et al. 2001). Reflection Grating Spectrometers (RGS den Herder et al. 2001) are located behind two of the telescopes while the 30-cm optical monitor (OM) instrument has its own optical/UV telescope (Mason et al. 2001). Data were reduced using the *XMM-Newton* Science Analysis System (SAS version 13.5).

The EPIC-PN instrument accumulated 0.4–15 keV photons in a *full frame* mode. In this mode, all pixels of all CCDs are read out and thus the full field of view is covered ($\sim 26 \times 26$ arcmin). The highest possible time resolution in this mode is 73.4 ms. We used concatenated and calibrated EPIC event lists available in the PPS Pipeline Products to generate light curves at different energy. We restricted the useful PN events to those with a pattern in the range 0 to 4 (single and doubles) and complying with the more strict selection criterion FLAG=0, which omits parts of the detector area like border pixels and columns with higher offset. After filtering, the effective exposure was 27 ks. The source region is free of pile-up as demonstrated by the fact that the observed distribution of counts as a function of the PI channel of single and double events agrees with the expected one. Using the SAS task *epatplot* we find that the 0.5 - 2.0 keV observed-to-model singles and doubles pattern fractions ratios are consistent with 1.0 within statistical errors (0.992 ± 0.027 and 1.011 ± 0.038 for single and double events, respectively).

To generate the light curves and spectrum, we extracted events from a circular region with radius 40 arcsec. To select the background region, we generated a list of all the detected sources in the PN field of view with the SAS task *edetect_chain* and chose a source-free region of the same size ~ 2.5 arcmin away from the source.

We mainly used data from the EPIC-PN camera because it is the instrument with the highest effective area. Nevertheless, because the count rate below ~ 1 keV was very low, we combined data from all three EPIC cameras for the analysis at low energies, including the search for pulsations and generation of pulse profile in the energy range 0.3–1 keV, and the better constraint of the uncertainties in the parameters of the soft spectral component.

2.2 Optical spectra

A long-term optical study of the donor star in IGR J21343+4738 has been presented in Reig & Zezas (2014). Here we present new optical spectroscopic observations that demonstrate the absence of

stars are normal Be stars seen nearly edge on, that is, with inclination angles $i \approx 90^\circ$ (Porter 1996).

Table 1. H α equivalent width measurements (1σ errors).

Date	Julian date (2,400,000+)	EW(H α) (Å)	Telescope
04-01-2013	56297.57	-2.1 ± 0.2	FLW
18-10-2013	56584.31	$+2.1 \pm 0.2$	SKO
03-11-2013	56599.63	$+2.1 \pm 0.2$	FLW
08-12-2013	56634.61	$+2.6 \pm 0.2$	FLW

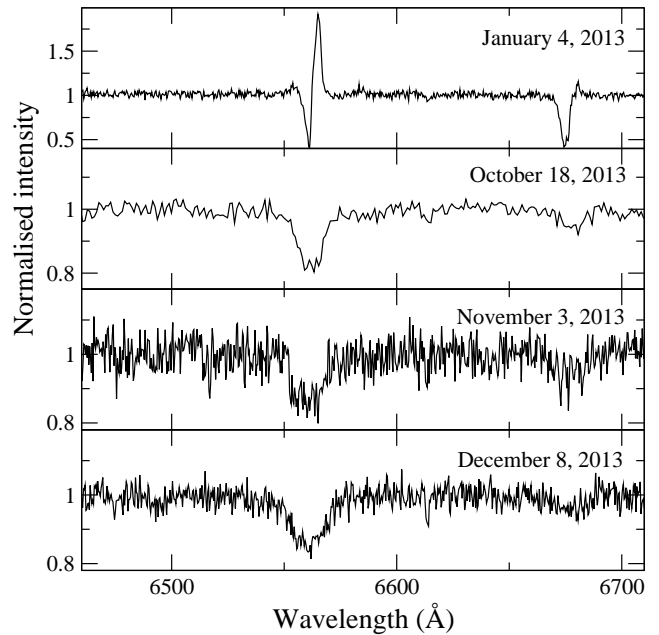


Figure 1. H α line profile. The *XMM-Newton* observations took place in November 24, 2013.

optical emission at the time of the X-ray observations. The dominant formation process of the hydrogen emission lines is recombination of the stellar flux by the disc. Thus, in the absence of the disc, no emission should be observed and the line should display the normal photospheric absorption profile. By convention, the equivalent width of an emission line is negative, while a positive value indicates an absorption profile. Although there is no optical observation at the exact time of the *XMM-Newton* observation, an absorption profile is observed 15–20 days before and after. This time is not enough for a disc to form. The formation and dissipation of a circumstellar disc in Be stars happen on timescales of months to years (Jones, Sigut & Porter 2008).

The optical spectra were obtained from the Skinakas observatory (SKO) in Crete (Greece) on the night October 18, 2013 and from the Fred Lawrence Whipple observatory (FLWO) at Mt. Hopkins (Arizona) on the night November 3, 2013 and December 8, 2013. We have also included our last observation in which the star was seen with the H α line in emission. The 1.3 m telescope of the Skinakas Observatory was equipped with a 2000 \times 800 (15 μ m) pixel ISA SITE CCD and a 1302 l mm⁻¹ grating, giving a nominal dispersion of ~ 1 Å/pixel. The FLW observations were made with the 1.5-m telescope, 1200 l mm⁻¹ grating and the FAST-II spectrograph (Fabricant et al. 1998).

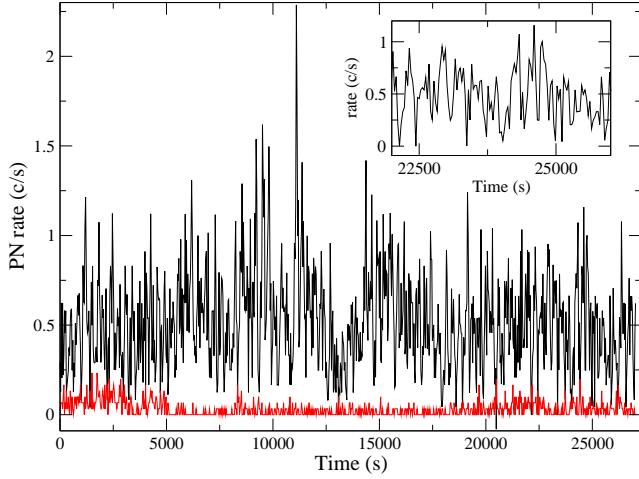


Figure 2. Background subtracted EPIC-PN light curve (black) and background light curve (red) in the energy range 0.2–12 keV with time bin of 30 s. The inset shows the pulsed nature of the X-ray emission.

Table 1 gives the log of the spectroscopic observations and the value of the $H\alpha$ equivalent width. Fig. 1 shows the line profiles.

3 RESULTS

3.1 Timing analysis and detection of X-ray pulsations

The PN light curve with 30 s time resolution in the energy range 0.2–12 keV is shown in Fig. 2 for the entire duration of the observation and for a shorter interval (see inset), where the presence of pulsed emission can be seen. In addition to the pulsations, the X-ray light curve shows moderate variability on time scales of a few ks. The root-mean-square measured in the 30 s binned light curve is $44 \pm 2\%$. The average source count rate after background subtraction is 0.517 ± 0.005 counts s^{-1} . The average background rate for the entire 27 ks observation is 0.033 ± 0.001 counts s^{-1} , but it is about 35% higher at the beginning of the observation owing to enhanced flaring particle background. If the first 5000 s of data are removed, then the average background count rate reduces to 0.024 ± 0.001 counts s^{-1} .

The timestamps of each event were corrected to the Earth’s barycenter prior to the extraction of the light curves from the event file. To search for periodic signal, we generated a 0.2–12 keV light curve with a time resolution of 1 s. Then we run a fast Fourier transform (FFT) algorithm to produce a single Leahy-normalized (Leahy et al. 1983) power spectrum covering the frequency interval $3.05 \times 10^{-5} - 0.5$ Hz in 16384 bins (Fig. 3). The maximum power is distributed over two bins at a frequency 0.003128052 Hz, which corresponds to a periodic signal with a period of ~ 320 s. Another strong peak is seen at twice this frequency and correspond to the first harmonic of the signal. The dashed line in the upper panel of Fig. 3 represents the $\sim 10\sigma$ detection level.

In addition, we also searched for periodic signal using an epoch-folding technique where the data is folded over a period range (Leahy 1987; Larsson 1996). For each trial period the χ^2 statistic is calculated. If the data contain a periodic signal, then a peak stands out in the $\chi^2 - P_{\text{trial}}$ plot. We used the task *efsearch* of the XRONOS package and found a best-fit period at 320.4 ± 0.1 s (Fig 3, lower panel).

To improve the estimation of the pulse period, we next ap-

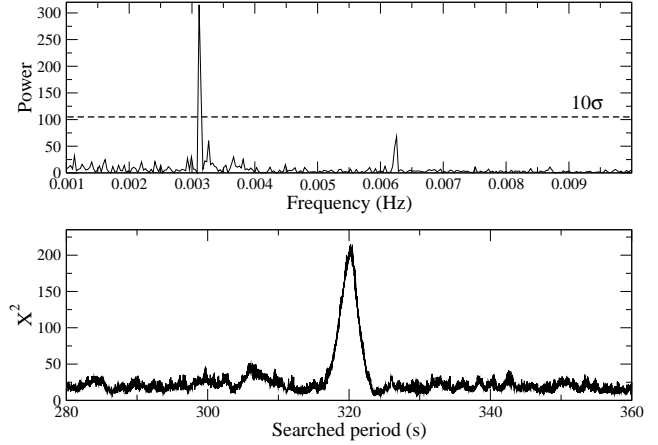


Figure 3. Upper panel: the EPIC-PN power spectrum and $\sim 10\sigma$ significance level. Lower panel: χ^2 maximization after folding the data over a range of periods (epoch folding).

Table 2. PN best-fit spectral parameters. A single power law (PL) and a power law plus a blackbody (BB) were considered. Errors correspond to 90% confidence. Quoted luminosity for an assumed distance of 8.5 kpc.

Parameter	Best-fit value (PL+BB)	Best-fit value (PL)
N_H	1.08 ± 0.15	0.63 ± 0.06
kT_{BB} (keV)	0.11 ± 0.01	–
Photon index	1.02 ± 0.07	0.85 ± 0.05
$F_{0.2-12\text{keV}}^{\text{unabs}}$ (erg $\text{cm}^{-2} \text{s}^{-1}$)	1.4×10^{-11}	5.8×10^{-12}
$L_{0.2-12\text{keV}}^{\text{unabs}}$ (erg s^{-1})	1.2×10^{35}	5.0×10^{34}
$L_{0.2-12\text{keV}}^{\text{abs}}$ (erg s^{-1})	4.4×10^{34}	4.5×10^{34}
χ^2/dof	1.13/111	1.39/113

plied a phase fitting technique. We divided the light curve into 8 segments, each of one with a length equal to 10 pulse periods and calculated a folded pulse profile for each segment with a common epoch and period. These profiles were cross-correlated with a template obtained by folding the entire light curve onto the trial period. The resulting phase delays were fitted with a linear function, whose slope provides the correction needed to be apply to the trial period. We then adjusted the period and repeated the procedure until the phase delay exhibited no net trend with time throughout the observation. The best-fit period was 320.35 ± 0.06 s, where the error was estimated from the uncertainty on the first-order term of a linear fit to the phase delays.

The pulse profiles obtained by folding light curves at different energy with the best-fit period are shown in Fig. 4. The profile exhibits a peak at the pulse maximum at low energies that disappears at high energies. At $\gtrsim 4$ keV the pulse maximum is flat. The pulse fraction, defined as $PF = (I_{\text{max}} - I_{\text{min}})/(I_{\text{max}} + I_{\text{min}})$, where I_{min} and I_{max} are background-corrected count rates at the pulse profile minimum and maximum, is $75 \pm 15\%$ below 1 keV but remains constant within the errors above that energy at a level of $45 \pm 3\%$.

3.2 Spectral analysis

We extracted a PN energy spectrum using the same source and background regions as for the timing analysis and filtering crite-

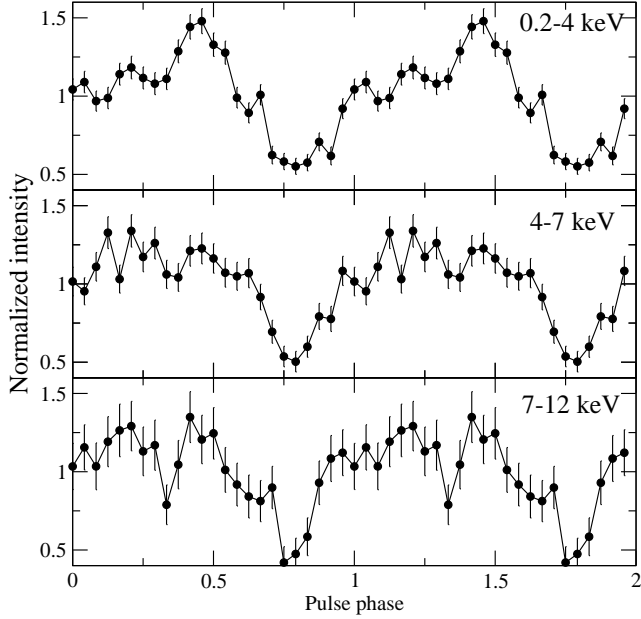


Figure 4. Normalized pulse profiles at different energies.

ria described. For the spectral analysis we further cleaned the data by accepting only the good times when sky background was low. In particular, the first ~ 5000 seconds of the observations, when enhanced background is observed, were discarded. We rebinned the energy spectra by requiring at least 50 counts for each energy bin.

A single component model composed of an absorbed power-law does not provide a satisfactory fit ($\chi^2 = 157$ for 113 degrees of freedom), leaving a deficit of flux at around 1.6 keV and weak soft excess below 1 keV (see Fig. 5). The addition of a blackbody component reduces significantly the amplitude of these two features and improves significantly the fit ($\chi^2 = 125$ for 111 degrees of freedom). Table 2 summarises the results of the spectral fit. The column density was obtained assuming abundances given in Anders & Grevesse (1989) and cross-sections from Balucinska-Church & McCammon (1992), with improvements from Yan, Sadeghpour & Dalgarno (1998).

However, the normalization of the blackbody component is poorly constrained (relative error of $\sim 50\%$). Leaving only the normalization of the blackbody and power law components free and fixing the rest of the parameters to their best-fit values, the uncertainty in the blackbody normalization goes down to $\sim 15\%$. In an attempt to better constrain the parameters of the blackbody component, we combined the spectra of all the EPIC cameras into a single spectrum. The best-fit parameters agree well with those obtained from the PN spectrum alone within errors, namely $N_H = (1.2 \pm 0.1) \times 10^{22} \text{ cm}^{-2}$, $kT = 0.10 \pm 0.01 \text{ keV}$, and $\Gamma = 1.10 \pm 0.05$. In this case, the uncertainty in the blackbody normalization reduces to 9% and the reduced $\chi^2_r = 1.06$, for 484 degrees of freedom.

In a paper devoted to cross-calibration of X-ray instruments, Tsujimoto et al. (2011, see Fig. 15) found excess of emission below 1.5 keV in the *XMM-Newton*/PN spectrum of the calibrating source G21.5-0.9. The origin of this feature is unknown. Although there are important differences² between G21.5-0.9 and

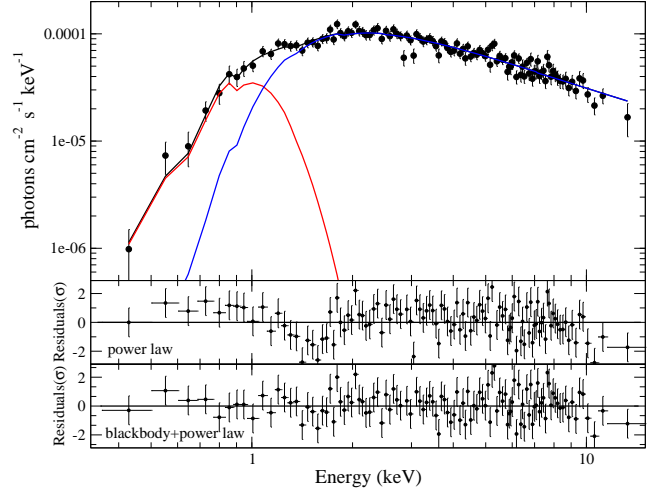


Figure 5. PN spectrum of IGR J21343+4738 (circles) and best-fit model (black line), which consists of a blackbody (red line) and a power law (blue line) components. The middle panel represents the residuals in terms of sigmas without the blackbody component. The bottom panel gives the residuals when the blackbody component is added to the fit.

IGR J21343+4738, the significance of the blackbody component should be treated with caution.

We found no evidence for an iron line emission line. The upper limit on the equivalent width of a 6.4 keV emission line is 28 eV.

The absorption significantly affects the shape of the spectrum below ~ 2 keV. The absorbed and unabsorbed X-ray fluxes in the 0.2–12 keV energy range are $5.1 \times 10^{-12} \text{ erg cm}^{-2} \text{ s}^{-1}$ and $1.4 \times 10^{-11} \text{ erg cm}^{-2} \text{ s}^{-1}$, respectively, whereas these fluxes for the 2–10 keV energy range are $3.8 \times 10^{-12} \text{ erg cm}^{-2}$ and $4.1 \times 10^{-12} \text{ erg cm}^{-2}$, respectively. Assuming a distance of 8.5 kpc (Reig & Zezas 2014), these values correspond to an absorbed and unabsorbed luminosities of $4.4 \times 10^{34} \text{ erg s}^{-1}$ and $1.2 \times 10^{35} \text{ erg s}^{-1}$, respectively, in the 0.2–12 keV band. In the case of the single power-law model, the column density is lower and the unabsorbed luminosity is $5.0 \times 10^{34} \text{ erg s}^{-1}$. Extra uncertainty in the luminosity comes from the uncertainty in the distance estimation. Taking all this into account, we conclude that the X-ray luminosity ranges between $(0.5 - 1.5) \times 10^{35} \text{ erg s}^{-1}$. Fig. 5 shows the PN spectrum and best fit, together with the residuals with (bottom panel) and without (middle panel) the addition of the blackbody component.

4 DISCUSSION

We have performed an X-ray timing and spectral analysis of IGR J21343+4738 and shown for the first time that the X-ray emission is pulsed with a pulse period of 320 s and a pulse fraction of $\sim 45\%$. Although the X-ray information of IGR J21343+4738 is scarce, the discovery of coherent X-ray pulsations is a key element to understand the nature of the system. Most X-ray pulsars are in high-mass X-ray binaries. The association of the X-ray source IGR J21343+4738 with a Be star, initially suspected by Bikmaev et al. (2008) has been firmly confirmed by Reig & Zezas (2014), who suggested a $V = 14.1$ B1Ive shell star located

² The calibrating source G21.5-0.9 is an extended X-ray source that fell in more than one PN chip. The background and chip gap correction issues do not affect IGR J21343+4738. Likewise, the instrumental effect appears to

peak at above 1 keV, whereas the soft excess in IGR J21343+4738 becomes apparent below 1 keV.

at a distance of ~ 8.5 kpc as the most likely optical counterpart. Virtually all BeXBs harbour accretion-powered pulsars. Thus the discovery of X-ray pulsations reinforces the membership of IGR J21343+4738 to the group of BeXB. However, the orbital period of IGR J21343+4738 remains unknown. According to the $P_{\text{spin}} - P_{\text{orb}}$ relationship (Corbet 1984), a $P_{\text{spin}} = 320$ s implies that an orbital period in the range 200–300 days should be expected. Such a long orbital period and most likely persistent X-ray emission at a level of $\lesssim 10^{35}$ erg s $^{-1}$ require the orbit to be nearly circular and accretion to occur via wind material from the massive companion in a similar fashion to the sub-class of BeXB suspected to be born with a smaller kick velocity ($\lesssim 50$ km s $^{-1}$) after the supernova explosion that gave birth to the neutron star. The characteristic of this sub-class of BeXBs has been studied by Pfahl et al. (2002). A natural consequence of a wide and circular orbit is the formation of extended and large circumstellar discs because the neutron star would not truncate the disc until it grows to a certain size. Thus, large $H\alpha$ equivalent widths should be expected in this type of systems. Indeed, members of this subclass of BeXB, such as X-Per, GS 0834–43, KS 1947+300, and 1RXS J225352.8+624354 have $H\alpha$ equivalent widths, $\text{EW}(H\alpha) \gtrsim -15$ Å (Clark et al. 2001; Israel et al. 2000; Negueruela et al. 2003; Esposito et al. 2013). In contrast, the maximum $\text{EW}(H\alpha)$ measured in IGR J21343+4738, in observations spaced by several years, is -8 Å (Reig & Zezas 2014). This weak $H\alpha$ emission points to a small and compact circumstellar disc, which could be the result of truncation by the neutron star. Truncation would require a narrower orbit and a shorter orbital period than those observed in the near-circular orbit systems.

Although IGR J21343+4738 is a variable source, it has not so far shown large type II outbursts as in BeXBs transients with much faster rotating neutron star such as 4U 0115+65 (Li, Wang & Zhao 2012; Müller et al. 2013) or V 0332+54 (Tsygankov, Lutovinov & Serber 2010; Nakajima, Mihara & Makishima 2010). In fact, the *Chandra* detection (Sazonov et al. 2008) when the source was thought to be in an off-state (below the threshold of the *INTEGRAL* instrument) suggests the possibility that IGR J21343+4738 is a persistent source. IGR J21343+4738 could be similar to the BeXB SAX J2103.5+4545, which also displays weak $H\alpha$ emission — the maximum $\text{EW}(H\alpha)$ ever reported is only ~ -5 Å (Reig et al. 2010). SAX J2103.5+4545 has a spin period of 355 seconds (Hulleman, in 't Zand & Heise 1998) and an orbital period of 12.7 days (Baykal, Stark & Swank 2000) and shows extended bright and faint X-ray states that last for a few hundred days (Reig et al. 2010). During the bright states, the neutron star spins up (Baykal et al. 2007; Camero Arranz et al. 2007), shows moderate type I outbursts modulated by the orbital period (Baykal, Stark & Swank 2000; Sidoli et al. 2005), and displays enhanced optical emission, characterised by $H\alpha$ line emission (Kızıloğlu et al. 2009; Reig et al. 2010). During the faint state, the modulation of the X-ray intensity with orbital phase disappears (Baykal, Stark & Swank 2002; Blay et al. 2004), the spin frequency of the neutron star remains fairly constant (Baykal et al. 2007) or slightly decreases, i.e., it spins down (Ducci et al. 2008) and the B-type companion shows $H\alpha$ in absorption (Kızıloğlu et al. 2009; Reig et al. 2010). The average X-ray luminosity in the low X-ray state of SAX J2103.5+4545 is $L_X \lesssim 10^{35}$ erg s $^{-1}$ in the 3–30 keV range. In short, the X-ray (long-period pulsations, bright and faint states, very weak iron emission line) and optical (small $\text{EW}(H\alpha)$, fast spectral changes) variability of IGR J21343+4738 resembles that of the persistent source SAX J2103.5+4545.

Our *XMM-Newton* observations of IGR J21343+4738 took

place during a low optical state, when the $H\alpha$ line was in absorption, implying the disappearance of the Be star's circumstellar disc (Fig. 1). The source has been in this state over more than six months (Reig & Zezas 2014). All spectra taken from June to December 2013 show an absorption profile. Without the disc, accretion should cease because the material in the disc constitutes the fuel that powers the X-ray emission. Still, pulsations are clearly detected, indicating that the accretion mechanism remains active. The measured X-ray luminosity is comparable to other persistent BeXB and well above the minimum luminosity at which the propeller effect sets in. For IGR J21343+4738, using equation (1) in Campana et al. (2002) and the canonical mass and radius of a neutron star and a typical magnetic field of 2×10^{12} G, we obtain $L_{\text{min}} = 2.2 \times 10^{32}$ erg s $^{-1}$. In the absence of the disc, X-rays could result from accretion from a stellar wind. Even though the wind from a main-sequence star is not as powerful as in a supergiant star, a narrow and eccentric orbit could in principle explain the observed luminosity, as it has been proposed for SAX J2103.5+4545 (Reig et al. 2005).

Assuming that all the gravitational energy is converted into X-rays, the X-ray luminosity powered by the stellar wind is given by (see e.g. Waters et al. 1989)

$$L_{\text{wind}} \approx 4.8 \times 10^{37} \left(\frac{M_X}{1.4 M_\odot} \right)^3 \left(\frac{R_X}{10^6 \text{ cm}} \right)^{-1} \left(\frac{M_*}{1 M_\odot} \right)^{-2/3} \left(\frac{P_{\text{orb}}}{1 \text{ day}} \right)^{-4/3} \left(\frac{\dot{M}_*}{10^{-6} M_\odot \text{ yr}^{-1}} \right) \left(\frac{v_w}{10^8 \text{ cm s}^{-1}} \right)^{-4} \text{ erg s}^{-1} \quad (1)$$

where M_X and R_X are the mass and radius of the neutron star, M_* and \dot{M}_* the mass and mass loss rate of the optical companion, P_{orb} the orbital period of the binary, and v_w the stellar wind velocity. The wind parameters of main-sequence Be stars are rather uncertain. Typical parameters for an early-type Be star are $M_* \sim 12 M_\odot$, $\dot{M}_* \sim (2-5) \times 10^{-8} M_\odot \text{ yr}^{-1}$, $v_w \sim (0.8-1) \times 10^8 \text{ cm s}^{-1}$ (Prinja 1989). However, these wind velocities were derived from ultraviolet observations, hence represent polar wind velocities. Infrared observations give a different picture and support the existence of a lower-velocity higher density equatorial wind, where the wind velocities are of the order of 150–600 km s $^{-1}$ and mass-loss rates an order of magnitude higher (Waters et al. 1988).

Assuming a mass-loss rate in the range $\dot{M}_* \sim (1-9) \times 10^{-8} M_\odot \text{ yr}^{-1}$, a velocity typical of the equatorial wind, $\sim 300-500$ km s $^{-1}$ would reproduce the observed unabsorbed X-ray luminosity of 10^{35} erg s $^{-1}$ in IGR J21343+4738. However, this would imply that the disc has not completely vanished, in contradiction with the profile of the $H\alpha$ line. This apparent contradiction can be solved taking into account the formation loci of the different observables in Be stars. Models of gaseous discs in Be stars show that disc emission only fills in the photospheric absorption profile when the disc size is about 5 stellar radii (Carciofi 2011). Thus even if an absorption profile is seen, a small disc might still be present. Two interesting facts support the presence of a small disc. First, the typical $H\alpha$ equivalent width for a normal (non-emitting) early-type B stars is about +3.5 Å (Jaschek & Jaschek 1987), whereas the measured equivalent width in IGR J21343+4738 is well below +3 Å, suggesting a small amount of fill-in emission. Second, the $H\alpha$ line shape of the October and November 2013 spectra (Fig. 1) is reminiscent of the so-called central (quasi)-emission peak profile, which appear when the innermost regions of the disc are being supplied with matter (Rivinius, Štefl & Baade 1999). Such a disc must be small and tenuous because no iron line at 6.4 keV is detected. This line results from reprocessing of the X-ray continuum in relatively cool matter and it is a very common if not ubiquitous feature in BeXB

(Reig & Nespoli 2013). Its detection provides strong evidence for the presence of material in the vicinity of the X-ray source.

The 0.2–12 keV spectrum of IGR J21343+4738 is well represented by a power law model and a blackbody component affected by photoelectric absorption. The blackbody component accounts for the excess of emission $\lesssim 1$ keV. Soft excess is a common feature observed in many, probably all, accreting X-ray pulsars (Hickox, Narayan & Kallman 2004; Mukherjee & Paul 2005; La Palombara & Mereghetti 2006, 2007; La Palombara et al. 2009). Hickox, Narayan & Kallman (2004) showed that when the soft excess is modelled with a blackbody component, the blackbody spectral parameters (temperature and emission radius) strongly depend on the source luminosity, which in turn, depends on the accretion mechanism. In high-luminosity pulsars, such as SMC X-1, Cen X-3 and LMC X-4, accretion occurs via Roche lobe overflow and an accretion disc is formed. In these systems $kT \approx 0.1$ keV and $R_{bb} \approx 1000$ km, typically, and the soft excess is believed to be due to reprocessing of hard X-rays in the inner parts of an accretion disc. Low-luminosity pulsars have $kT \approx 1 - 1.5$ keV and $R_{bb} \approx 0.1$ km. In these systems the soft excess would be originated at the base of the accretion column, close to the neutron star surface. The wind-fed supergiant systems have $kT \approx 0.2$ keV and $R_{bb} \approx 60 - 100$ km. In these systems, the thermal component responsible for the soft excess is likely to be a cloud of diffuse plasma around the neutron star. In IGR J21343+4738, the best-fit gives a blackbody temperature and radius of the emitting region³ are $kT = 0.11 \pm 0.01$ K and $R_{bb} = 80 \pm 15$ km, for a distance of 8.5 kpc. The emitting region responsible for the soft excess in IGR J21343+4738 is too large to come from the polar cap of the neutron star and too small to come from the inner parts of an accretion disc. The radius of the accreting polar cap is estimated as $R_{cap} \approx R_X(R_X/R_m)^{1/2}$, where R_m is the radius of the magnetosphere, which for the case of IGR J21343+4738, i.e. assuming $L_X = 1 \times 10^{35}$ erg s⁻¹ and a typical magnetic moment of 10^{30} G cm³, is $R_m = 1.4 \times 10^9$ cm. Thus $R_{cap} \sim 0.27$ km. On the other hand, the inner parts of an accretion disc would be outside the magnetosphere (> 14000 km). The fact that pulsations are still detected below ~ 1 keV indicates that the blackbody emitting region is phase locked with the neutron star.

An alternative source of matter during the absence of the circumstellar wind might be a residual accretion disc around the neutron star as has been suggested for the BeXB 1A 0535+262 Doroshenko et al. (2014), based on the similarity of the spectral and timing properties of the quiescent and outburst X-ray emission. Because there is evidence that an accretion disc is present in 1A 0535+262 during outbursts, the similarities suggest a common origin of the quiescent and bright X-ray emission. Given that no X-ray outburst has been seen in IGR J21343+4738, no such comparison is possible. Note however, that the absence of the iron emission line argues against large amount of matter (e.g. an accretion disc) in the vicinity of the system.

When only high-energy data from *INTEGRAL* was available, IGR J21343+4738 was seen to go through on- and off X-ray states as many other transient Be/X-ray pulsars. The *INTEGRAL* luminosity during the active states was comparable to the one detected by *XMM-Newton* in this work, namely in the order of 10^{35} erg s⁻¹. The *Chandra* detection when the source was in an off state and the *XMM-Newton* observation during a dis-loss episode

suggest that IGR J21343+4738 is a persistent source. Moreover, the lack of large amplitude X-ray intensity variability (no giant X-ray outbursts typical of transient systems have been seen in IGR J21343+4738) and the lack of a strong iron line are also characteristics of persistent BeXB (Reig & Roche 1999). Nevertheless, the number of X-ray observations of IGR J21343+4738 is still very limited and larger amplitude increases of X-ray intensity in the form of outbursts cannot be ruled out. An example of a persistent BeXB which suddenly exhibited enhanced X-ray activity is RX J0440.9+4431 (Ferrigno et al. 2013).

5 CONCLUSION

We have performed the first detailed X-ray timing and spectral analysis of the Be/X-ray binary IGR J21343+4738 and found that its X-ray emission pulses with a pulse period of 320 s. The X-ray observation took place at a time when the B star companion had (almost) lost the circumstellar disc, which it is assumed to be the prime source of matter that powers the X-ray through accretion. Despite this low-optical state, the X-ray luminosity is comparable to that seen in other persistent Be/X-ray binaries with discs and significantly larger than the minimum luminosity at which accretion is expected to halt due to the centrifugal inhibition caused by the propeller effect. We argue that a equatorially enhanced stellar wind could explain the observed luminosity. The X-ray spectrum shows a soft excess, whose origin is not clear. If it is modeled with a blackbody, then the size of the emitting region is not compatible neither with the polar cap nor the inner parts of an accretion disc.

ACKNOWLEDGMENTS

This work has made use of NASA's Astrophysics Data System Bibliographic Services and of the SIMBAD database, operated at the CDS, Strasbourg, France.

REFERENCES

- Anders E., Grevesse N., 1989, *Geochim. Cosmochim. Acta*, 53, 197
- Balucinska-Church M., McCammon D., 1992, *ApJ*, 400, 699
- Baykal A., Inam S. Ç., Stark M. J., Heffner C. M., Erkoca A. E., Swank J. H., 2007, *MNRAS*, 374, 1108
- Baykal A., Stark M. J., Swank J., 2000, *ApJ*, 544, L129
- Baykal A., Stark M. J., Swank J. H., 2002, *ApJ*, 569, 903
- Bikmaev I. F., Burenin R. A., Revnivtsev M. G., Sazonov S. Y., Sunyaev R. A., Pavlinsky M. N., Sakhibullin N. A., 2008, *Astronomy Letters*, 34, 653
- Bird A. J. et al., 2007, *ApJS*, 170, 175
- Blay P., Reig P., Martínez Núñez S., Camero A., Connell P., Reglero V., 2004, *A&A*, 427, 293
- Camero Arranz A., Wilson C. A., Finger M. H., Reglero V., 2007, *A&A*, 473, 551
- Campana S., Stella L., Israel G. L., Moretti A., Parmar A. N., Orlandini M., 2002, *ApJ*, 580, 389
- Carciofi A. C., 2011, in *IAU Symposium*, Vol. 272, IAU Symposium, Neiner C., Wade G., Meynet G., Peters G., eds., pp. 325–336
- Clark J. S., Tarasov A. E., Okazaki A. T., Roche P., Lyuty V. M., 2001, *A&A*, 380, 615
- Corbet R. H. D., 1984, *A&A*, 141, 91

³ The normalization of the blackbody component is $N = R_{bb}^2/D_{10}^2$, where R_{bb} is the source radius in km, and D_{10} is the distance to the source in units of 10 kpc.

- den Herder J. W. et al., 2001, *A&A*, 365, L7
- Doroshenko V., Santangelo A., Doroshenko R., Caballero I., Tsygankov S., Rothschild R., 2014, *A&A*, 561, A96
- Ducci L., Sidoli L., Paizis A., Mereghetti S., Pizzochero P. M., 2008, in *Proceedings of the 7th INTEGRAL Workshop*
- Esposito P., Israel G. L., Sidoli L., Mason E., Rodríguez Castillo G. A., Halpern J. P., Moretti A., Götz D., 2013, *MNRAS*, 433, 2028
- Fabricant D., Cheimets P., Caldwell N., Geary J., 1998, *PASP*, 110, 79
- Ferrigno C., Farinelli R., Bozzo E., Pottschmidt K., Klochkov D., Kretschmar P., 2013, *A&A*, 553, A103
- Hickox R. C., Narayan R., Kallman T. R., 2004, *ApJ*, 614, 881
- Hulleman F., in 't Zand J. J. M., Heise J., 1998, *A&A*, 337, L25
- Israel G. L. et al., 2000, *MNRAS*, 314, 87
- Ives J. C., Sanford P. W., Bell Burnell S. J., 1975, *Nature*, 254, 578
- Jansen F. et al., 2001, *A&A*, 365, L1
- Jaschek C., Jaschek M., 1987, *The classification of stars*
- Jones C. E., Sigut T. A. A., Porter J. M., 2008, *MNRAS*, 386, 1922
- Kızıloğlu Ü., Özbilgen S., Kızıloğlu N., Baykal A., 2009, *A&A*, 508, 895
- Krivosos R., Revnivtsev M., Lutovinov A., Sazonov S., Churazov E., Sunyaev R., 2007, *A&A*, 475, 775
- La Palombara N., Mereghetti S., 2006, *A&A*, 455, 283
- La Palombara N., Mereghetti S., 2007, *A&A*, 474, 137
- La Palombara N., Sidoli L., Esposito P., Tiengo A., Mereghetti S., 2009, *A&A*, 505, 947
- Larsson S., 1996, *A&AS*, 117, 197
- Leahy D. A., 1987, *A&A*, 180, 275
- Leahy D. A., Darbro W., Elsner R. F., Weisskopf M. C., Kahn S., Sutherland P. G., Grindlay J. E., 1983, *ApJ*, 266, 160
- Li J., Wang W., Zhao Y., 2012, *MNRAS*, 423, 2854
- Mason K. O. et al., 2001, *A&A*, 365, L36
- Mukherjee U., Paul B., 2005, *A&A*, 431, 667
- Müller S. et al., 2013, *A&A*, 551, A6
- Nakajima M., Mihara T., Makishima K., 2010, *ApJ*, 710, 1755
- Negueruela I., Israel G. L., Marco A., Norton A. J., Speziali R., 2003, *A&A*, 397, 739
- Parkes G. E., Murdin P. G., Mason K. O., 1980, *MNRAS*, 190, 537
- Pfahl E., Rappaport S., Podsiadlowski P., Spruit H., 2002, *ApJ*, 574, 364
- Porter J. M., 1996, *MNRAS*, 280, L31
- Prinja R. K., 1989, *MNRAS*, 241, 721
- Reig P., 2011, *Ap&SS*, 332, 1
- Reig P., Negueruela I., Papamastorakis G., Manousakis A., Kougentakakis T., 2005, *A&A*, 440, 637
- Reig P., Nespoli E., 2013, *A&A*, 551, A1
- Reig P., Roche P., 1999, *MNRAS*, 306, 100
- Reig P., Słowikowska A., Zezas A., Blay P., 2010, *MNRAS*, 401, 55
- Reig P., Zezas A., 2014, *ArXiv e-prints*
- Rivinius T., Štefl S., Baade D., 1999, *A&A*, 348, 831
- Sazonov S., Revnivtsev M., Burenin R., Churazov E., Sunyaev R., Forman W. R., Murray S. S., 2008, *A&A*, 487, 509
- Sidoli L. et al., 2005, *A&A*, 440, 1033
- Staubert R., Pottschmidt K., Doroshenko V., Wilms J., Suchy S., Rothschild R., Santangelo A., 2011, *A&A*, 527, A7
- Strüder L. et al., 2001, *A&A*, 365, L18
- Tsujimoto M. et al., 2011, *A&A*, 525, A25
- Tsygankov S. S., Lutovinov A. A., Serber A. V., 2010, *MNRAS*, 401, 1628
- Turner M. J. L. et al., 2001, *A&A*, 365, L27
- Waters L. B. F. M., de Martino D., Habets G. M. H. J., Taylor A. R., 1989, *A&A*, 223, 207
- Waters L. B. F. M., van den Heuvel E. P. J., Taylor A. R., Habets G. M. H. J., Persi P., 1988, *A&A*, 198, 200
- Yan M., Sadeghpour H. R., Dalgarno A., 1998, *ApJ*, 496, 1044